Journal of Molecular Modeling (2024) 30:423
https://doi.org/10.1007/s00894-024-06205-7

ORIGINAL PAPER

Exploring wide gap semiconductor characteristics in α-pinene crystals: insights from density functional theory

T. A. Santos[1] · R. B. Marques[2] · A. M. Silva[3] · E. P. S. Martins[3] · L. A. Ribeiro Júnior[4] · M. L. Pereira Júnior[5] · A. Macedo-Filho[1,6]

Received: 25 March 2024 / Accepted: 1 November 2024 / Published online: 30 November 2024

Abstract

Context α-Pinene, a bicyclic monoterpene found extensively in the essential oils of conifers, has shown potential in pharmacological applications. This study theoretically investigates the structural and electronic properties of the (1*S*)-(−)-α-pinene crystal, focusing on its potential for nanoelectronic applications due to the observed wide band gap. Structural analysis revealed that the crystal's unit cell contains 104 atoms with orthorhombic symmetry, and its lattice parameters show excellent agreement with experimental data. Electronic analysis indicated an indirect band gap of 3.58 eV for LDA-PZ and 4.32 eV for GGA-PBE, suggesting that (1*S*)-(−)-α-pinene behaves as a wide band-gap semiconductor. The electronic structure is primarily influenced by contributions from the p_y orbitals of Carbon atoms and the *s* orbital of Hydrogen atoms, highlighting potential sites for chemical interaction.

Methods DFT calculations were performed using the Quantum Espresso software. They employed both the local density approximation (LDA-PZ) and the generalized gradient approximation (GGA-PBE), parameterized by the Perdew-Burke-Ernzerhof exchange-correlation functional. Norm-conserving pseudopotentials were applied to represent the core electrons accurately.

Keywords Structural properties · Electronic structure · DFT calculations · Semiconductor materials · α-Pinene

Introduction

Terpenes, a diverse class of secondary metabolites, are widely distributed in various plant species, comprising one of the largest natural compound classes, with approximately 55,000 isolated members documented [1]. Terpene cyclase enzymes play a crucial role in converting simple, linear hydrocarbon phosphates into a diverse array of chiral, carbocyclic chains [2, 3]. The pharmaceutical significance of terpenes is linked to essential oils, intricate mixtures of volatile secondary metabolites, predominantly monoterpenes, sesquiterpenes, phenylpropanoids, alcohols, ethers, aldehydes, and ketones [4]. Essential oils exhibit considerable structural diversity and possess diverse biological activities, including anti-inflammatory, antioxidant, anti-neoplastic, and antimicrobial properties [4–9].

This study emphasizes α-pinene ($C_{10}H_{16}$), a pivotal member of the terpene family, present in leaf oils of various plants such as *Croton heliotropiifolius Kunth* [7] and numerous coniferous trees [9, 10]. α-Pinene, existing in enantiomeric forms 1 S,5 S- or (−)-α-pinene and 1R,5R- or (+)-α-pinene, as well as (+)-β-pinene and (−)-β-pinene [11], demonstrates versatility by transforming into various terpenes, expanding its range of applications [9, 12–15].

Given the considerable interest in the potential applications of α-pinene, particularly in the realm of nanotechnology and nanoelectronic devices [16, 17], this study employs

✉ M. L. Pereira Júnior
marcelo.lopes@unb.br

1 PPGQ-GERATEC, State University of Piauí, 64002-150 Teresina, PI, Brazil

2 Biotechnology and Biodiversity Research Center, State University of Piauí, 64260-000 Teresina, PI, Brazil

3 Campus Prof. Antonio Geovanne Alves de Sousa, State University of Piauí, 64260-000 Piripiri, PI, Brazil

4 University of Brasília, Institute of Physics, 70910-900 Brasília, DF, Brazil

5 Department of Electrical Engineering, University of Brasília, Faculty of Technology, 70910-900 Brasília, DF, Brazil

6 Department of Physics, State University of Piauí, 64002-150 Teresina, PI, Brazil

density functional theory (DFT) to investigate the structural and electronic properties of the (1*S*)-(−)-α-pinene crystal [18–20]. Our goal is to contribute to the understanding of its electronic behavior, aligning with similar studies on organic crystals, such as amino acids and DNA bases, which have exhibited semiconductor characteristics [21–26].

In the following sections, we detail our computational approach in the "Methodology" section, outlining the implementation of the DFT methodology. The "Results" section presents our calculations and discussions, shedding light on our investigative efforts. Finally, the "Conclusions" section encapsulates our conclusions, underscoring the relevance of understanding the electronic properties of organic crystals like α-pinene for the development of sustainable and biocompatible nanoelectronic systems [22, 27, 28].

Methodology

The Quantum Espresso (QE) software, an open-source code developed by Giannozzi et al., was utilized for conducting our Density Functional Theory (DFT) calculations [29–32]. In this study, we employed the Local Density Approximation - Perdew-Zunger (LDA-PZ) and Generalized Gradient Approximation - Perdew-Burke-Ernzerhof (GGA-PBE) exchange-correlation functionals to account for exchange-correlation interactions [33, 34]. The LDA-PZ calculations incorporated the use of norm-conserving pseudopotentials [35–37].

For the GGA-PBE approach, the size of the analyzed structure necessitated the adoption of the ultra-soft pseudopotential (USPP) type. This choice facilitated calculations with the lowest possible cutoff energy for the plane-wave basis set. Crystal geometry optimization was executed using the variable unit cell relaxation calculation (vc-relax) implemented in the QE code. This involved determining lattice parameters, angles, and atomic positions by searching for a total energy minimum. A self-consistent field (SCF) convergence threshold of 10^{-8} served as the criterion for convergence in these optimizations. The kinetic-energy cutoff for LDA-PZ and GGA-PBE calculations was set at $50Ry$ ($\sim 680.3eV$) and $40Ry$ ($\sim 544.2eV$), respectively, with a Monkhorst-Pack grid of $4 \times 4 \times 4$ for both cases.

Additionally, we employed the ORCA (version 5.0) computational program package, a quantum chemistry tool featuring various electronic structure methods such as DFT, many-body perturbation, coupled cluster theories, and multireference and semiempirical methods [38]. Specifically, ORCA was utilized to optimize the gas phase of (−)-α-pinene, aiming to obtain the frontier molecular orbital, electrical charge per atom through Mulliken's and Hirshfeld's electronic population analysis, and the electrostatic potential. Single-point calculations were performed using LDA (defaults to VWN5), GGA-PBE functionals, and basis sets def2-TZVP and def2/J [39, 40].

Results

Structural properties

The unit cell of the (1*S*)-(−)-α-pinene crystal is depicted in Fig. 1, illustrating the first Brillouin zone. Comprising four molecules of ($H_{10}C_{16}$), the crystal possesses a total of 104 atoms in its unit cell. The lattice parameters are $a = 7.1944(6)$Å, $b = 7.5920(3)$Å, $c = 15.9190(15)$Å, with angles $\alpha = \beta = \gamma = 90°$ and a volume $V = 869.49(11)$Å^3. This crystal exhibits orthorhombic symmetry within the space group $P2_1P2_1P2_1(Z = 4)$ [41–44].

LDA-PZ and GGA-PBE calculations provided lattice parameters (a, b, c) and volume (V), presented in Table1. Our theoretical calculations reveal a decrease, denoted as Δ, in the order of $\Delta a = -0.7726$Å, $\Delta b = -0.7763$Å, $\Delta c = -1.8489$Å, and $\Delta V = -253.65$Å^3 for the LDA-PZ approach. Conversely, GGA-PBE calculations resulted in an increase of $\Delta a = 0.4430$Å, $\Delta b = 0.2456$Å, $\Delta c = 0.6819$Å, and $\Delta V = 147.01$Å^3 compared to experimental data. No significant deviations in the angles α, β, and γ were observed.

Examining atomic positions, LDA-PZ calculations highlight the largest deviations in the x-coordinate of $H19$, y-coordinate of $H55$, and z-coordinate of $H86$, with $\Delta x = -1.0399$Å, $\Delta y = -1.1411$Å, and $\Delta z = -2.1296$Å, respectively. For the GGA-PBE approach, the x-coordinate of $C60$, y-coordinate of $H70$, and z-coordinate of $H6$ exhibit the largest deviations, albeit not exceeding 0.70Å. Overall,

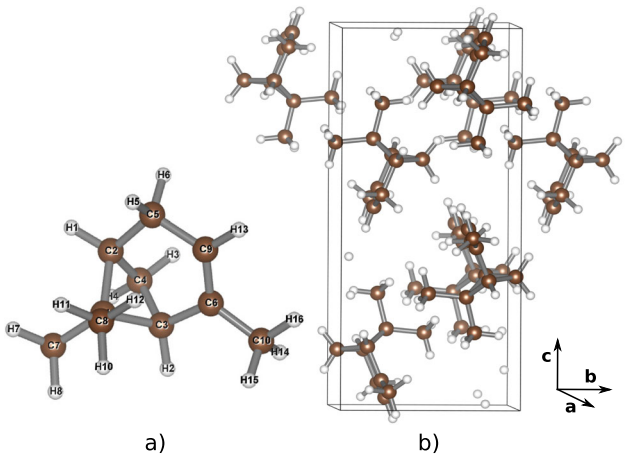

Fig. 1 **a** Three-dimensional structure of the (−)-α-pinene molecule. Brown spheres represent carbon atoms, and white spheres represent hydrogen atoms. **b** (1*S*)-(−)-α-pinene crystal, consisting of four molecules ($H_{10}C_{16}$) in its unit cell, with lattice parameters $a = 7.1944(6)$Å, $b = 7.5920(3)$Å, $c = 15.9190(15)$Å, $\alpha = \beta = \gamma = 90°$, and volume $V = 869.49(11)$Å^3 [41]

Table 1 (1*S*)-(−)-α-pinene lattice parameters

C. Level	a [Å]	Δa [Å]	b [Å]	Δb [Å]	c [Å]	Δc [Å]	V [Å^3]	ΔV [Å^3]
Exp. [41]	7.1944(6)	–	7.5920(3)	–	7.5920(3)	–	869.49(11)	–
LDA-PZ	6.4218	−0.7726	6.8157	−0.7763	6.8157	−0.7763	615.84	−253.65
GGA-PBE	7.6374	0.4430	8.0176	0.4256	8.0176	0.4256	1016.54	147.01

our results indicate good agreement between the theoretical approach and the experimentally reported structural parameters [41–44], supporting the subsequent analysis of the electronic properties of the (1*S*)-(−)-α-pinene crystal.

Electronic properties

Kohn-Sham's electronic band structure describes the electronic eigenenergies $E_n(\vec{k})$ based on a set of quantum numbers that compose the components of a wave vector $\vec{k}$ at the first Brillouin zone [22]. Here, the integer n signifies the number of bands. Usually, the eigenenergies are obtained along a path that contains a set of high-symmetry points. In this study, we considered Γ(0, 0, 0), X(0.5, 0, 0), S(0.5, 0.5, 0), Y(0, 0.5, 0), Z(0, 0, 0.5), U(0.5, 0, 0.5), R(0.5, 0.5, 0.5), and T(0, 0.5, 0.5) as the high-symmetry points employed for our calculations. The schematic path in the Brillouin zone used for the band structure calculations of the (1*S*)-(−)-α-pinene crystal is shown in Fig. 2. The arrows linking each high-symmetry point indicate the high-symmetry paths, as follows: Γ-X-S-Y-Γ-Z-U-R-T-Z.

Figure 3a and c show the optimized electronic band structures of the (1*S*)-(−)-α-pinene. LDA-PZ and GGA-PBE calculations close to the main energy band-gap depict the most relevant electronic transitions between the top valence band (VB) and the conduction band (CB). In both calculations, the maximum of the VB is located at the Γ high-symmetry point, while the minimum of the CB is at the *Y* high-symmetry point. For LDA-PZ calculations, we observe an indirect transition with an energy band-gap of about $3.58eV$ along the intermediate point next to Γ to Y high-symmetry point, followed by secondary indirect gaps of $3.59eV$ and $3.60eV$ along the Γ → T and Z → Y paths, respectively. Regarding GGA-PBE, we observe an indirect

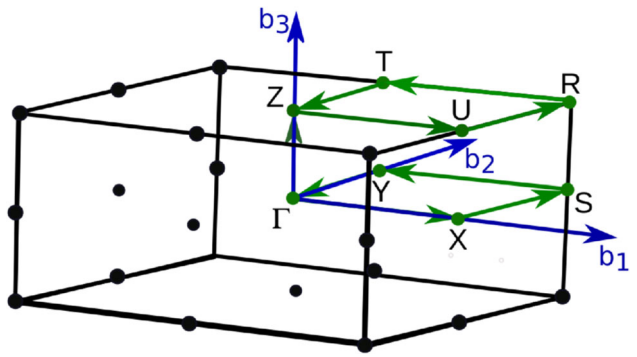

Fig. 2 First Brillouin Zone of the orthorhombic structure of the (1*S*)-(−)-α-pinene crystal. High-symmetry paths employed to obtain the electronic band structure are pointed out. Γ(0, 0, 0), X(0.5, 0, 0), S(0.5, 0.5, 0), Y(0, 0.5, 0), Z(0, 0, 0.5), U(0.5, 0, 0.5), R(0.5, 0.5, 0.5), and T(0, 0.5, 0.5) are the high-symmetry points, obeying the Γ-X-S-Y-Γ-Z-U-R-T-Z steps

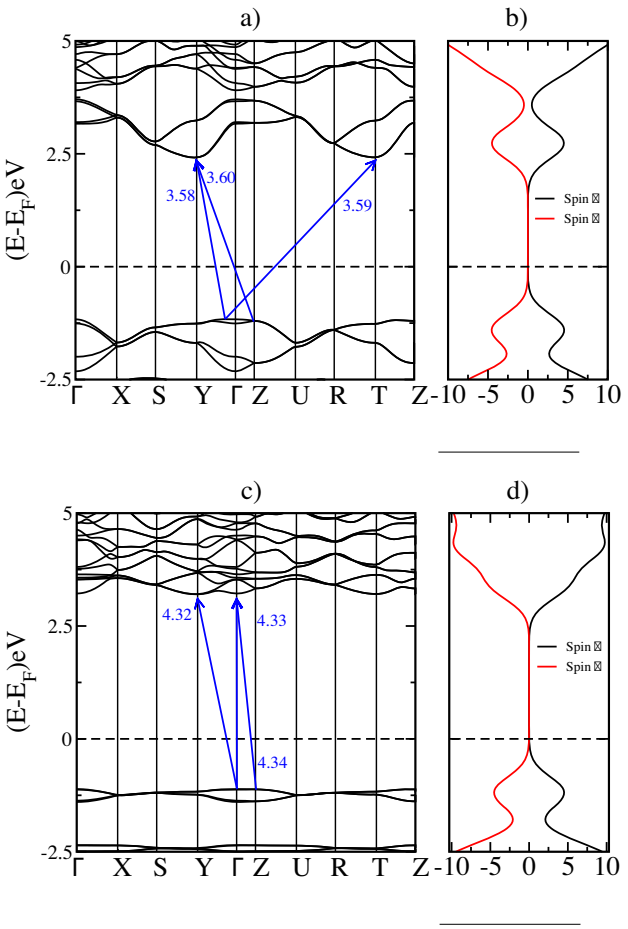

Fig. 3 (Color online) Electronic band structure calculations for the (1*S*)-(−)-α-pinene crystal. **a** provides LDA-PZ calculations showing the main indirect transition with an energy band-gap of about $3.58eV$, followed by secondary indirect gaps of $3.59eV$ and $3.60eV$. **b** shows DOS calculations, indicating that the spin presents a symmetric behavior. **c** shows GGA-PBE calculations, indicating a main indirect band-gap at about $4.32eV$ from Γ to *Y* high-symmetry point. A secondary direct gap of about $4.33eV$ (Γ → Γ) is observed, followed by another secondary indirect gap around $4.34eV$ (Z → Γ). The dashed black line is the Fermi level deviated to zero

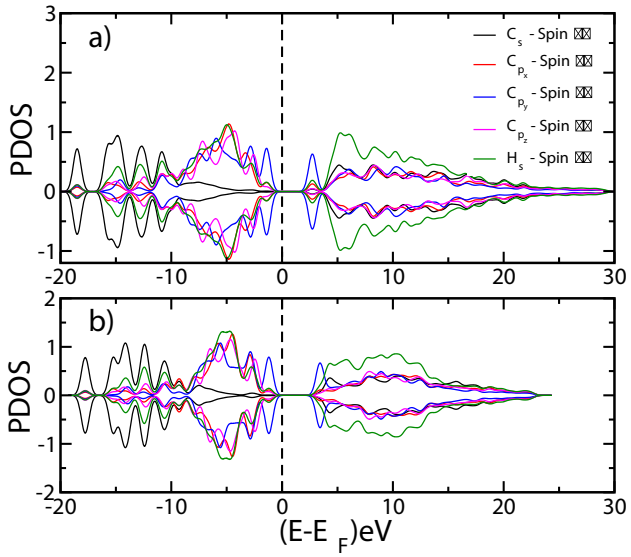

Fig. 4 (Color online) Projected density of state (PDOS) of the (−)-α-pinene molecule. Both calculations were evaluated and optimized for the LDA-PZ and GGA-PBE functionals. Here, it is possible to observe the partial contribution of the s and p (p_x, p_y, and p_z) orbitals of the Carbon atom and the s orbital of the Hydrogen atom. The dashed black line is the Fermi level deviated to zero

transition with an energy band-gap of about $4.32eV$ along the $\Gamma \rightarrow Y$ path, followed by a secondary direct gap of about $4.33eV$ ($\Gamma \rightarrow \Gamma$) and another secondary indirect gap around $4.34eV$ ($Z \rightarrow \Gamma$). Additionally, Fig. 3b and d show the electronic density of state (DOS) for both LDA-PZ and GGA-PBE. The black and red lines (spin up and down) follow the energy band structure and present symmetric behavior along the broad energy spectrum.

Next, Fig. 4a and b show the projected electronic density of state (PDOS) for the (−)-α-pinene molecule. Here, we observe the partial contribution of the s and p (p_x, p_y, and p_z) orbitals of the Carbon atom and the s orbital of the Hydrogen atom. In both cases (LDA-PZ and GGA-PBE), near the VB and CB, the significant contribution in the electronic transition is the p_y of the Carbon orbital, followed by the s orbital of the Hydrogen atom. Each orbital behaves symmetrically along the broad energy spectrum, as indicated by the contribution of spins up and down.

Figure 5 shows the frontier molecular orbital of the (−)-α-pinene molecule, displaying the overall behavior of the molecular orbitals from Homo-4 to Lumo+4 for both LDA and GGA-PBE functionals (Fig. 5a and b, respectively). Table 2 presents the energy values corresponding to each Homo and Lumo specified. The LDA calculations furnished the Homo-Lumo energy gap at about $4.78eV$, while GGA-PBE furnished $4.83eV$. A small gap between Lumo and Lumo+1 is observed at about $0.76eV$ ($0.78eV$) for LDA (GGA-PBE), respectively, facilitating a possible electronic transition. Despite the implications of this Homo-Lumo gap, the results align with the previous finding that the (1S)-(−)-α-pinene crystal behaves like a wide band-gap semiconductor material. The molecular boundary orbitals HOMO and LUMO can be crucial for biological interactions between ligands and proteins [45–49].

Table 3 presents the electrical charge per atom calculated from Mulliken's and Hirshfeld's electronic population analysis, expressed in elementary charge unit e. LDA(GGA-PBE) analysis reveals that the electronic charge distributions are mostly related to the carbon atoms, where LDA furnishes, for the Mulliken's (Hirshfeld's) charge, a resultant value of about $-2.300e$ ($-0.526e$). In comparison, GGA-PBE calculations furnish, for Mulliken's (Hirshfeld's) charge, a resultant value of about $-1.902e$ ($-0.435e$). The differences among the positive and negative Mulliken's (Hirshfeld's) charges indicate $0.003e$ ($0.000e$) and $0.001e$ ($0.003e$) for LDA and GGA-PBE, respectively. These findings suggest a dipolar behavior of the zwitterionic state inside the (1S)-(−)-α-pinene crystal [23, 24, 50, 51]. Additionally, Fig. 6 displays the electronic density along the (−)-α-pinene molecule. Both LDA and GGA-PBE calculations indicate a similar distribution of electronic charges, aligning with the results from Mulliken's and Hirshfeld's charge population analysis. The region with higher electronic density, represented by a higher concentration of negative charge (red), is observed for the

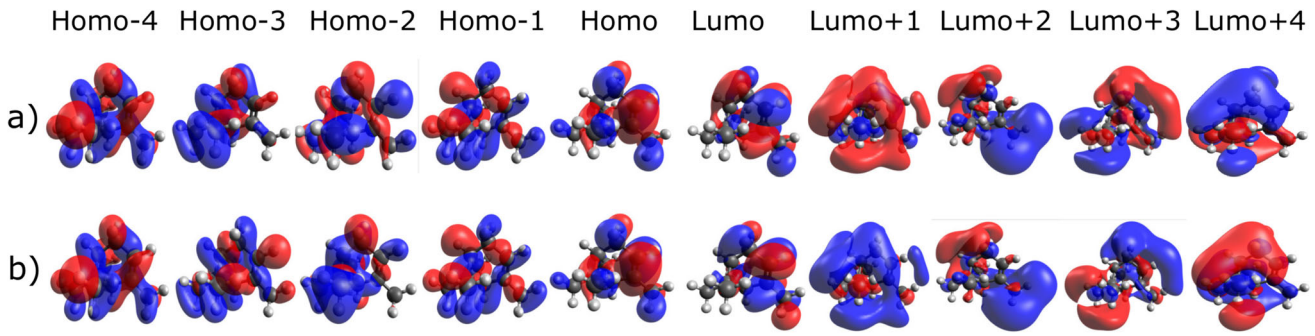

Fig. 5 (Color online) Overall behavior of the frontier molecular orbital of the (−)-α-pinene molecule. Both calculations were performed employing **a** LDA and **b** GGA-PBE functionals

Table 2 Homo and Lumo energies (eV) of the frontier molecular orbital of the (−)-α-pinene molecule, varying from Homo-4 through Lumo+4

C. Level	Homo-4	Homo-3	Homo-2	Homo-1	Homo	Lumo	Lumo+1	Lumo+2	Lumo+3	Lumo+4
LDA	−7.89	−7.10	−7.08	−6.63	−5.44	−0.66	0.10	0.81	0.98	1.09
GGA-PBE	−7.75	−6.99	−6.98	−6.53	−5.31	−0.48	0.30	0.94	1.13	1.25

electronic density of the carbon atoms along the ring that constitutes the molecule, indicating sites with a higher probability of chemical interactions, as described in molecular docking studies [45, 47].

Conclusions

In conclusion, this study presents a comprehensive theoretical investigation of α-pinene, an organic compound within the terpene family, utilizing first-principles calculations. Our focus extended to exploring the structural and electronic properties of the (1S)-(−)-α-pinene crystal and its constituent molecule. Notably, our calculated structural parameters align closely with experimental observations.

The outcomes of our investigation reveal distinctive electronic band structures for the (1S)-(−)-α-pinene crystal, providing insights into its behavior. LDA-PZ calculations unveil an indirect transition featuring an energy band-gap of approximately $3.58eV$. This transition occurs along an intermediate path from Γ to Y high-symmetry points, with subsequent secondary indirect gaps measuring $3.59eV$ and $3.60eV$ along the Γ → T and Z → Y trajectories, respectively.

On the other hand, GGA-PBE calculations showcase an indirect transition with an energy band-gap of about $4.32eV$ along the Γ → Y path. This is succeeded by a secondary direct gap of approximately $4.33eV$ (Γ → Γ) and another secondary indirect gap of around $4.34eV$ (Z → Γ). Notably, the density of states (DOS) analysis illustrates symmetric behavior between spin up and down along the broad energy spectrum, indicating an absence of magnetization properties in the (1S)-(−)-α-pinene crystal.

A parallel observation is made for the projected density of states (PDOS) obtained from the (−)-α-pinene molecule. The analysis highlights the distinct contributions of the s and p orbitals of the Carbon atom, including p_x, p_y, and p_z, along with the s orbital of the Hydrogen atom. Moreover, the Homo-Lumo gap derived from the (−)-α-pinene molecule aligns with the wide band-gap semiconductor behavior observed in the (1S)-(−)-α-pinene crystal. These findings underscore the potential relevance of (1S)-(−)-α-pinene in nanoelectronic applications.

Table 3 Mulliken and Hirshfeld electronic population analysis (e) of the (1S)-(−)-α-pinene molecule evaluated and optimized for the LDA and GGA-PBE functionals

Atoms	LDA		GGA-PBE	
	Mulliken	Rirshfeld	Mulliken	Rirshfeld
1C	−0.110	+0.013	+0.015	+0.022
2C	−0.080	−0.023	+0.087	−0.015
3C	−0.050	−0.027	+0.192	−0.019
4C	−0.197	−0.062	−0.269	−0.053
5C	−0.239	−0.057	−0.163	−0.045
6C	+0.016	−0.004	−0.080	+0.002
7C	−0.427	−0.095	−0.373	−0.081
8C	−0.439	−0.102	−0.381	−0.088
9C	−0.250	−0.063	−0.210	−0.056
10C	−0.508	−0.093	−0.426	−0.078
11 H	+0.106	+0.028	+0.062	+0.022
12 H	+0.116	+0.029	+0.072	+0.023
13 H	+0.118	+0.028	+0.080	+0.021
14 H	+0.143	+0.030	+0.093	+0.024
15 H	+0.156	+0.035	+0.097	+0.028
16 H	+0.145	+0.036	+0.093	+0.028
17 H	+0.151	+0.031	+0.109	+0.025
18 H	+0.152	+0.031	+0.109	+0.025
19 H	+0.142	+0.031	+0.108	+0.026
20 H	+0.145	+0.031	+0.102	+0.025
21 H	+0.150	+0.031	+0.105	+0.025
22 H	+0.177	+0.025	+0.138	+0.021
23 H	+0.114	+0.032	+0.080	+0.026
24 H	+0.163	+0.038	+0.122	+0.031
25 H	+0.161	+0.039	+0.121	+0.032
26 H	+0.148	+0.038	+0.118	+0.032

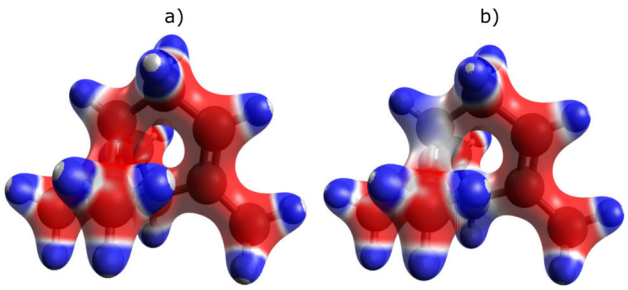

Fig. 6 (Color online) Electrostatic potential for the (−)-α-pinene molecule. **a** LDA and **b** GGA-PBE functionals show a similar distribution of the electronic charge. Red indicates negative charge, and blue indicates positive charge. LDA(GGA-PBE) analysis reveals that the electronic charge distributions are mostly related to the carbon atoms

Acknowledgements This work received partial support from Brazilian agencies CAPES, CNPq, and FAPDF. L.A.R.J. acknowledges CAPES for partially financing this study — Finance Code 88887.691997/2022-00. CENAPAD-SP (Centro Nacional de Alto Desenpenho em São Paulo - Universidade Estadual de Campinas – UNICAMP) provided computational support for L.A.R.J. and M.L.P.J. (proj634, and proj960). L.A.R.J. thanks the financial support from Brazilian Research Council FAP-DF grant 00193.00001808/2022-71, FAPDF-PRONEM grant 00193.00001247/2021-20, 00193-00001857/2023-95, 00193-00001782/2023-42, and CNPq grants 350176/2022-1. M.L.P.J. acknowledges the financial support from FAP-DF grant 00193-00001807/2023-16. L.A.R.J and M.L.P.J. also thanks Núcleo de Computação de Alto Desempenho (NACAD) for computational facilities through the Lobo Carneiro Supercomputer. A.M.F. gratefully acknowledges the support from Conselho Nacional de Desenvolvimento Científico (CNPq), grants 459961/2014 − 4 and 424950/2018 − 9. We acknowledge the Laboratório de Física Teórica e Modelagem Computacional (LFTMC) for providing the computational facilities.

Author contribution T.A.S., R.B.M.., A.M.S., and E.P.S.M.: data curation, formal analysis, methodology, writing—original draft preparation. M.L.P.J. and L.A.R.J.: funding acquisition and writing—reviewing and editing. A.M.F.: data curation, formal analysis, methodology, funding acquisition, conceptualization, and writing—reviewing and editing. All authors reviewed the manuscript.

Availability of data and material All data generated or analyzed during this investigation are included in this published article.

Declarations

Conflict of interest The authors declare no competing interests.

References

1. Ninkuu V, Zhang L, Yan J, Fu Z, Yang T, Zeng H (2021) Biochemistry of terpenes and recent advances in plant protection. Int J Mol Sci 22(11):5710. https://doi.org/10.3390/ijms22115710
2. Maimone T, Baran P (2007) Modern synthetic efforts toward biologically active terpenes. Nat Chem Biol 3:396. https://doi.org/10.1038/nchembio.2007.1
3. Chen K, Baran P (2009) Total synthesis of eudesmane terpenes by site-selective c-h oxidations. Nat Lett 459:824. https://doi.org/10.1038/nature08043
4. Bakkali F, Averbeck S, Averbeck D, Idaomar M (2008) Biological effects of essential oils - a review. Food Chem Toxicol 46:446–475. https://doi.org/10.1016/j.fct.2007.09.106
5. Ji HF, Li XJ, Zhang HY (2009) Natural products and drug discovery. EMBO Rep 10:194. https://doi.org/10.1038/s41573-020-00114-z
6. Jucá D, da Silva M, Junior RJ, de Lima F, Okoba W, Lahlou S, de Oliveira R, dos Santos A, Magalhães P (2011) The essential oil of eucalyptus tereticornis and its constituents, α- and β-pinene, show accelerative properties on rat gastrointestinal transit. Planta Med 77:57–59. https://doi.org/10.1055/s-0030-1250116
7. Marques R et al (2023) Pharmacokinetic and toxicological prediction of the chemical constituents of the essential oil of the leaves of croton heliotropiifolius kunth. J Toxicol Environ Health, Part A 1–12. https://doi.org/10.1080/15287394.2023.2216734
8. Chen W et al (2015) Anti-tumor effect of α-pinene on human hepatoma cell lines through inducing g2/m cell cycle arrest. J Pharmacol Sci 127:332–333. https://doi.org/10.1016/j.jphs.2015.01.008
9. Kim DS et al (2015) Alpha-pinene exhibits anti-inflammatory activity through the suppression of mapks and the nf-κb pathway in mouse peritoneal macrophages. Am J Chin Med 43:731–742. https://doi.org/10.1142/S0192415X15500457
10. de Groot A, Schmidt E (2016) Essential oils. Part III: chemical composition. Dermatitis 27:161–169. https://doi.org/10.1201/9781003204350
11. Noma Y, Asakawa Y (2010) In: Liu HWB, Mander L (Eds) Comprehensive natural products II, (Elsevier), p 669–801. https://doi.org/10.1016/B978-008045382-8.00742-5
12. Farooq A et al (2002) Biotransformation of (−)-α-pinene by botrytis cinerea. Z Naturforsch C J Biosci 57:303. https://doi.org/10.1515/znc-2002-3-418
13. Yang J et al (2013) Metabolic engineering of escherichia coli for the biosynthesis of alpha-pinene. Biotechnol Biofuels 6:1–10. https://doi.org/10.1186/1754-6834-6-60
14. Waidyanatha S et al (2022) The common indoor air pollutant alpha-pinene is metabolised to a genotoxic metabolite alpha-pinene oxide. Xenobiotica 52:303–311. https://doi.org/10.1080/00498254.2022.2070047
15. Chiu C, Keeling C, Bohlmann J (2017) Toxicity of pine monoterpenes to mountain pine beetle. Sci Rep 7:1. https://doi.org/10.1038/s41598-017-08983-y
16. Yamusa SA, Shaari A, Isah I, Ibrahim UB, Kunya SI, Abdulkarim S, Itas Y, Alsalamh M (2023) Effects of exchange correlation functional (vwdf3) on the structural, elastic, and electronic properties of transition metal dichalogenides. J Niger Soc Phys Sci 1094–1094
17. Yamusa SA, Shaari A, Alsaif NA, Alsalamah IM, Isah I, Rekik N (2022) Elucidating the structural, electronic, elastic, and optical properties of bulk and monolayer mos2 transition-metal dichalcogenides: a DFT approach. ACS Omega 7(49):45719
18. Giustino F (2014) Materials modelling using density functional theory: properties and predictions. Oxford University Press, New York
19. Hernández B, Sanchez-Cortes S, Ghomi M (2023) Energetic, conformational and vibrational features of the tripeptide $(Gly)_3$: data from MP2 and DFT calculations. Comput Theor Chem 1220:113989. https://doi.org/10.1016/j.comptc.2022.113989
20. Banerjee P, Mukhopadhyay K (2023) Electronic, magnetic and optical properties of transition metal doped nd_2o_3: a DFT insight. Sci Rep 1220:114016. https://doi.org/10.1016/j.comptc.2022.114016
21. Caetano E et al (2018) Anhydrous proline crystals: structural optimization, optoelectronic properties, effective masses and Frenkel exciton energy. J Phys Chem Sol 121:36–47. https://doi.org/10.1016/j.jpcs.2018.08.011
22. Zanatta G et al (2014) L-asparagine crystals with wide gap semiconductor features: optical absorption measurements and density functional theory computations. J Chem Phys 140:124511. https://doi.org/10.1063/1.4869179
23. Silva AM et al (2012) Optical absorption and DFT calculations in l-aspartic acid anhydrous crystals: charge carrier effective masses point to semiconducting behavior. Phys Rev B 86. https://doi.org/10.1103/PhysRevB.86.195201
24. Pereira FAR, Macedo-Filho A, Silva AM et al (2023) On the structural, electronic, and optical properties of l-histidine crystal: a DFT study. J Mol Model 29(7):205. https://doi.org/10.1007/s00894-023-05580-x
25. Santos JGS, Macedo-Filho A, Silva AM et al (2021) Computational structural, electronic and optical properties of the palmitic acid in its c form. J Mol Model 27:145. https://doi.org/10.1007/s00894-021-04752-x
26. Maia JFF, Freire VN, Caetano EWS, Azevedo DL, Sales FAM, Albuquerque EL (2011) Anhydrous crystals of DNA bases are wide

gap semiconductors. J Chem Phys 134. https://doi.org/10.1063/1.3584680
27. Irimia-Vladu M, Saricifici NS, Bauer S (2001) Exotic materials for bioorganic electronic. J Mater Chem 21:1350. https://doi.org/10.1039/C0JM02444A
28. Parpura V (2012) Bionanoelectronics: getting close to the action. Nat Nanotechnol 7:143
29. Giannozzi P et al (2020) Quantum espresso toward the exascale. J Chem Phys 152:154105. https://doi.org/10.1063/5.0005082
30. Giannozzi P et al (2017) Advanced capabilities for materials modelling with quantum espresso. J Condens Matter Phys 29:465901. https://doi.org/10.1088/1361-648X/aa8f79
31. Giannozzi P et al (2009) Quantum espresso: a modular and open-source software project for quantum simulations of materials. J Condens Matter Phys 21:395502. https://doi.org/10.1088/0953-8984/21/39/395502
32. Nguyen TH, Nugraha ART, Saito R (2023) Quantum espresso course for solid-state physics. Jenny Stanford Publishing, Singapore
33. Perdew JP, Burke K, Ernzerhof M (1996) Generalized gradient approximation made simple. Phys Rev Lett 77:3865. https://doi.org/10.1103/PhysRevLett.77.3865
34. Perdew JP et al (1992) Atoms, molecules, solids, and surfaces: applications of the generalized gradient approximation for exchange and correlation. Phys Rev B 46:6671
35. Perdew JP, Zunger A (1981) Self-interaction correction to density functional approximations for many-electron systems. Phys Rev B 23:5048
36. Prassides K et al (1996) Isolation, structure, and electronic calculations of the heterofullerene salt $k_6c_{59}n$. Phys Rev B 271:1833. https://doi.org/10.1126/science.271.5257.1833
37. Andreoni W, Giannozzi P, Parrinello M (1995) Molecular structure and chemical bonding in k_3c_{60} and k_6c_{60}. Phys Rev B 51:287. https://doi.org/10.1103/physrevb.51.2087
38. Neese F (2012) The orca program system. Wires Comput Mol Sci 2:73. https://doi.org/10.1002/wcms.81
39. Li Y, Zeng P, Lou Q, Su X, Li W, Wang X (2024) Prediction of 19F NMR chemical shifts for organic compounds with ORCA. J Magn Reson 358:107611. https://doi.org/10.1016/j.jmr.2023.107611
40. Hu Y, Zhang Z, Huang L (2020) Quantum chemical calculations for elucidating chiral resolution mechanism of chiral covalent organic frameworks chromatographic stationary phase. Chin J Chromatogr 38(12):1449. https://doi.org/10.3724/sp.j.1123.2020.05009
41. Bond A, Davies J (2001) (1*s*)-(−)-α-pinene. Acta Crystallographica Section E E57:o1039–o1040. https://doi.org/10.1107/S1600536801016415
42. Deng Q, Jiang L, Yu Y, Yang Y (2022) Theoretical exploration of the mechanism of α-pinene hydrogenation. J Organomet Chem 980:122513
43. Liu P, Liu X, Saburi T, Kubota S, Huang P, Wada Y (2021) Thermal stability and oxidation characteristics of α-pinene, β-pinene and α-pinene/β-pinene mixture. RSC Adv 11(33):20529
44. Neeman EM, Avilés Moreno JR, Huet TR (2017) The gas phase structure of α-pinene, a main biogenic volatile organic compound. J Chem Phys 147(21)
45. Rocha JA et al (2018) Computational quantum chemistry, molecular docking, and ADMET predictions of imidazole alkaloids of Pilocarpus microphyllus with schistosomicidal properties. PLoS One 13(6):e0198476. https://doi.org/10.1371/journal.pone.0198476
46. Da Silva RR, Ramalho TC, Santos JM, Figueroa-Villar JD (2006) On the limits of highest-occupied molecular orbital driven reactions: the frontier effective-for-reaction molecular orbital concept. J Phys Chem 110:1031. https://doi.org/10.1021/jp054434y
47. Maltarollo VG, Silva DC, Honório KM (2012) Advanced QSAR studies on PPARδ ligands related to metabolic diseases. J Braz Chem Soc 23:85. https://doi.org/10.1590/S0103-50532012000100013
48. Pang X, Zhou L, Zhang M, Zhang L, Xu L, Xie F, Yu L, Zhang X (2012) Two rules on the protein-ligand interaction. Open Conf Proc J 3:70. https://doi.org/10.2174/2210289201203010070
49. Itoh Y, Nakashima Y, Tsukamoto S et al (2019) N+-c-h···o hydrogen bonds in protein-ligand complexes. Sci Rep 9:767. https://doi.org/10.1038/s41598-018-36987-9
50. Koerner MM, Palacio LA, Wright JW, Schweitzer KS, Ray BD, Petrache HI (2011) Electrodynamics of lipid membrane interactions in the presence of zwitterionic buffers. Biophys J 101:362. https://doi.org/10.1016/j.bpj.2011.05.062
51. Qian L, Liu W, Yang M, Nica V, Yang J, Liu H, Ning L, Zhang S, Zhang Q (2020) Zwitterionic polymer chain-assisted lysozyme imprinted core-shell carbon microspheres with enhanced recognition and selectivity. Talanta 217:121085. https://doi.org/10.1016/j.talanta.2020.121085